

A hydrodynamic study of hyperon spin polarization in relativistic heavy ion collisions

Baochi Fu,^{1,2} Kai Xu,^{1,2} Xu-Guang Huang,^{3,4,*} and Huichao Song^{1,2,5,†}

¹*Department of Physics and State Key Laboratory of Nuclear Physics and Technology, Peking University, Beijing 100871, China*

²*Collaborative Innovation Center of Quantum Matter, Beijing 100871, China*

³*Department of Physics and Center for Field Theory and Particle Physics, Fudan University, Shanghai, 200433, China*

⁴*Key Laboratory of Nuclear Physics and Ion-beam Application (MOE), Fudan University, Shanghai 200433, China*

⁵*Center for High Energy Physics, Peking University, Beijing 100871, China*

(Dated: January 7, 2022)

We perform a systematic study of the spin polarization of hyperons in heavy-ion collisions using the MUSIC hydrodynamic model with A Multi-Phase Transport (AMPT) pre-equilibrium dynamics. Our model calculations nicely describe the measured collision-energy, centrality, rapidity, and p_T dependence of Λ polarization. We also study and predict the global spin polarization of Ξ^- and Ω^- as a function of collision energy, which provides a baseline for the studies of the magnetic moment, spin, and mass dependence of the spin polarization. For the local spin polarization, we calculate the radial and azimuthal components of the transverse Λ polarization and find specific modulating behavior which could reflect the circular vortical structure. However, our model fails to describe the azimuthal-angle dependence of the longitudinal and transverse Λ polarization, which indicates that the hydrodynamic framework with the spin Cooper-Frye formula under the assumption of thermal equilibrium of spin degree of freedom needs to be improved.

I. INTRODUCTION

In peripheral high-energy heavy-ion collisions, the colliding system contains a large amount of orbital angular momentum perpendicular to the reaction plane, a portion of which is carried by the produced quark-gluon plasma (QGP) in the form of fluid vorticity. Such orbital angular momentum of QGP can be transferred into the spin of the constituent particles via the spin-vorticity coupling. As a results, the final emitted hyperons are globally spin-polarized along the direction of initial angular momentum [1, 2].

In experiments, the spin polarization of Λ and $\bar{\Lambda}$ hyperons (“ Λ polarization”) can be determined by measuring the angular distribution of their weak-decay products. In such a way, the global Λ polarization (i.e., the spin polarization integrated over kinematics) has been successfully observed by STAR Collaboration in 7.7- 200 A GeV Au + Au collisions at Relativistic Heavy Ion Collider(RHIC) [3–6], while was also reported to be consistent with zero in 2.76 A TeV and 5.02 A TeV Pb + Pb collisions at the Large Hadron Collider (LHC) [7]. Besides the global polarization, the differential Λ polarization has also been measured (dubbed local Λ polarization) [6–8]. In particular, it is found that the longitudinal component of Λ polarization shows a quadrupole pattern in the transverse plane[8]. Different from the global behavior, such quadrupole structure of the longitudinal Λ polarization survives at very high collision energies indicating that the spin polarization might be influenced by not only the initial orbital angular momentum but also other contributions like, e.g., the inhomogeneous expansion of the fireball.

In theory, the global spin polarization in heavy-ion collisions was first proposed by Liang and Wang [1] and was noted by Voloshin from the experimental side [2]. Early

works focused on calculations of spin polarization of quarks and anti-quarks and the polarization of final hadrons was estimated through recombination or fragmentation mechanism [1, 9–11]. Later on, an explicit formula, called spin Cooper-Frye formula, that connects the spin polarization of hadrons to the thermal vorticity at freeze-out hypersurface was established for the thermal equilibrium system [12] (see also Refs. [13, 14] for derivations in kinetic theory). It can be used to calculate Λ polarization with hydrodynamics or transport model simulations and roughly fit the global Λ polarization [15–25]. However, such spin Cooper-Frye formula fails to reproduce the azimuthal-angle dependence of Λ polarization and results in a sign difference compared with the experimental data [26–32]. (For reviews, please refer to Refs. [33–38].) Besides the Λ polarization, the spin polarization of quarks can also lead to other potential observables, such as the global and local spin alignment of vector mesons [39–42], enhancement of spinful hadrons’ yields [43], baryonic spin hall effect [44].

In this work, we perform a systematic study on the Λ polarization in 7.7 A GeV- 200 A GeV Au + Au collisions, using the MUSIC hydrodynamic model with A Multi-Phase Transport (AMPT) pre-equilibrium initial condition. Such hydrodynamic models and hybrid approaches have been widely used in relativistic heavy-ion collision at RHIC and the LHC energies, which successfully describe various soft hadronic observables such as the particle yields, transverse momentum spectra, flows anisotropies [45–56]. In hydrodynamic calculations, the dynamic variables are local temperature, flow velocity, and conserved charge densities. Using the spin Cooper-Frye formula, the spin polarization vector can be calculated with these hydrodynamics variables on the freeze-out surface. In [18, 20, 22], the energy dependence of global Λ polarization has been reproduced with hydrodynamic calculations. However, for the local Λ polarization, hydrodynamics fails to reproduce the sign of the azimuthal-angle dependence of both transverse and longitudinal polarization [18, 20, 26–28], which is a pending puzzle. In this work, we will fur-

* huangxuguang@fudan.edu.cn

† huichaosong@pku.edu.cn

ther study the global and local spin polarization within the AMPT+MUSIC hydrodynamic framework. For the global polarization, besides demonstrating that AMPT+MUSIC model can nicely describe the measured collision-energy, centrality, rapidity, and p_T dependence of Λ polarization, we will predict the spin polarization of Ξ^- and Ω^- , which provides a baseline for the studies of the magnetic moment, spin, and mass dependence of the spin polarization. For the local polarization, we focus on investigating how the initial condition and hydrodynamic evolution influence the local polarization and how different vorticity terms influence the local polarization of P_z . We also calculate the radial and azimuthal components of the transverse Λ polarization and find specific modulating behavior which could reflect the circular vortical structure.

This paper is organized as follows. Section II gives a brief introduction to AMPT+MUSIC hybrid model and the spin polarization formula used in this work. Section III presents and discusses the results of global and local spin polarization. Section IV concludes and summarizes the paper.

II. MODEL SETUP

In this work, we implement AMPT+MUSIC hybrid model to study the global and local Λ -polarization in 7.7- 200 A GeV Au + Au collisions at RHIC. AMPT is A Multi-Phase Transport Model developed in [57], which is implemented here to simulate the pre-equilibrium dynamics and generate the initial profiles for the succeeding MUSIC hydrodynamic evolution. MUSIC is a 3+1 dimensional relativistic viscous hydrodynamic model [46, 47, 58] to describe the evolution of the QGP fireball. The MUSIC hydrodynamics can also be followed by a UrQMD afterburner [59, 60] to describe the scattering and evolution of dilute hadronic matter.

Compared with early hybrid model simulations with AMPT initial energy density profiles [61–63], we generate the whole energy-momentum tensor $T^{\mu\nu}$ from AMPT for the hydrodynamic evolution since initial flow is essential for the development of fluid vorticity for the study of spin polarization.

A. AMPT Initial condition

In this paper, we use AMPT model to generate the initial energy-momentum tensor $T^{\mu\nu}$ and net baryon current N^μ for the succeeding MUSIC hydrodynamic evolution. In the string melting version of AMPT [57], the sub-program HIJING [64, 65] samples initial partons from mini-jets and excitation strings. Then, the phase-space information of partons is imported to sub-program ZPC for the subsequent partonic evolution. Here we do not evolve this partonic stage till hadronization but take the information of partons at a certain switching hypersurface with a constant proper time τ_0 (the initial time of hydrodynamics).

On the switching hypersurface, the energy-momentum tensor $T^{\mu\nu}$ and net baryon density n are constructed from Gaus-

sian smearing in Milne coordinate as [61, 66, 67]:

$$T^{\mu\nu}(\tau_0, x, y, \eta_s) = \sum_i \frac{p_i^\mu p_i^\nu}{p_i^\tau} \Phi_G(\tau_0, \mathbf{x}; \mathbf{x}_i), \quad (1a)$$

$$n(\tau_0, x, y, \eta_s) = \sum_i Q_i \Phi_G(\tau_0, \mathbf{x}; \mathbf{x}_i), \quad (1b)$$

where the smearing function Φ_G is given by

$$\Phi_G(\tau_0, \mathbf{x}; \mathbf{x}_i) = \frac{K}{\tau_0 \sqrt{2\pi\sigma_{\eta_s}^2}} \frac{1}{2\pi\sigma_r^2} \times \exp \left[-\frac{(x-x_i)^2 + (y-y_i)^2}{2\sigma_r^2} - \frac{(\eta_s - \eta_{is})^2}{2\sigma_{\eta_s}^2} \right]. \quad (2)$$

Here, p_i^μ denotes the 4-momentum vector of the i -th parton with $p_i^\tau = m_{iT} \cosh(Y_i - \eta_{is})$, $p_i^x = p_{ix}$, $p_i^y = p_{iy}$, $p_i^\eta = m_{iT} \sinh(Y_i - \eta_{is})/\tau_0$, m_{iT} the transverse mass, Y_i the rapidity, and η_{is} the spacetime rapidity of the i -th parton. Q_i is the baryon charge of i -th parton. The Gaussian smearing factors $\sigma_r, \sigma_{\eta_s}$, and scale factor K are tuned to fit the spectra and flow of all charged hadrons at the most central collisions and are kept fixed for other centrality classes (see also Refs. [61, 66]). In each centrality bin, we average 1,000 AMPT events to get smooth initial $T^{\mu\nu}$ and n profiles for the succeeding hydrodynamic evolution.

B. MUSIC Hydrodynamics

MUSIC is a 3+1 dimensional viscous hydrodynamic program which solves the conservation equations for energy momentum tensor $T^{\mu\nu}$ and charge current N^μ [45, 46, 58]:

$$\partial_\mu T^{\mu\nu}(x) = 0, \quad (3a)$$

$$\partial_\mu N^\mu(x) = 0, \quad (3b)$$

and the 2nd order Israel-Stewart equations for shear stress tensor $\pi^{\mu\nu}$ and bulk pressure Π [68, 69]:

$$\tau_\Pi \dot{\Pi} + \Pi = -\zeta\theta - \delta_{\Pi\Pi}\Pi\theta + \lambda_{\Pi\pi}\pi^{\mu\nu}\sigma_{\mu\nu}, \quad (4a)$$

$$\tau_\pi \dot{\pi}^{\langle\mu\nu\rangle} + \pi^{\mu\nu} = 2\eta\sigma^{\mu\nu} - \delta_{\pi\pi}\pi^{\mu\nu}\theta + \phi_\tau \pi_\alpha^{\langle\mu} \pi^{\nu\rangle\alpha} - \tau_{\pi\pi} \pi_\alpha^{\langle\mu} \sigma^{\nu\rangle\alpha} + \lambda_{\pi\Pi} \Pi \sigma^{\mu\nu}. \quad (4b)$$

Here, $T^{\mu\nu}$ and N^μ are decomposed as $T^{\mu\nu} = \epsilon u^\mu u^\nu - (p + \Pi)\Delta^{\mu\nu} + \pi^{\mu\nu}$, $N^\mu = n u^\mu$, where u^μ is the flow 4-velocity, ϵ is the local energy density, p is pressure, n is the net baryon density, and $\Delta^{\mu\nu} = g^{\mu\nu} - u^\mu u^\nu$ is the transverse projector to the flow velocity u^μ . In Eqs. (4), η and ζ are shear and bulk viscosities, $A^{\langle\cdots\rangle}$ is the symmetrized and traceless projection, $\theta = \nabla_\mu u^\mu$ and $\sigma^{\mu\nu} = \frac{1}{2}[\nabla^\mu u^\nu + \nabla^\nu u^\mu - \frac{2}{3}\Delta^{\mu\nu}(\nabla_\alpha u^\alpha)]$ with $\nabla_\mu = \Delta_{\mu\nu}\partial^\nu$. The transport coefficients τ_Π , $\delta_{\Pi\Pi}$, $\lambda_{\Pi\pi}$, τ_π , $\delta_{\pi\pi}$, ϕ_τ , $\tau_{\pi\pi}$ and $\lambda_{\pi\Pi}$ are fixed by the Boltzmann equations [69, 70]. Note that we have neglected the baryon diffusion effect in this study so that N^μ only contains the ideal part. To close the system, we input a crossover-type equation of state (EOS) as used in [54].

At the freeze-out hypersurface defined by a given constant energy density E_{sw} , various hadron resonances are generated

by the Monte-Carlo event generator iSS [71] according to the differential Cooper-Frye formula: [72]:

$$E \frac{dN_i}{d^3p}(x) = \frac{g_i}{(2\pi)^3} p \cdot d^3\Sigma(x) f_i(x, p), \quad (5)$$

where $f_i = f_{\text{eq},i}(x, p) + \delta f_i(x, p)$ is the distribution function of the particle species i with the equilibrium and off equilibrium parts taken the form $f_{\text{eq},i}(x, p) = \frac{1}{e^{[p \cdot u(x) + \mu_B]/T} + 1}$ and $\delta f_i(x, p) = f_{\text{eq},i}(x, p)(1 - f_{\text{eq},i}(x, p)) \frac{p^\mu p^\nu \pi^{\mu\nu}}{2T^2(\epsilon + P)}$ [71, 73].

With these emitted hadrons, the hydrodynamic evolution can be followed by the UrQMD [59, 60] to describe the scatterings and decays of dilute hadronic matter. After all the interactions cease, the information of these hadrons are taken to obtain various soft hadron observables.

Table I lists the parameter setups in our calculations. In more details, the specific shear viscosity η/s is set to be a constant and the specific bulk viscosity, ζ/s is taken a form with temperature dependence, which reach a peak near the phase transition as in Ref. [70]. Following Ref. [49], the initial time τ_0 of hydrodynamic evolution is set to be 0.4 fm/c for 200 A GeV Au+Au collisions and gradually increase to 2.0 fm/c for 7.7 A GeV Au+Au collisions. The switching energy density E_{sw} changes from 0.65 GeV/fm³ to 0.35 GeV/fm³, which roughly matches the chemical freeze-out temperature obtained from the statistical model from high to low collision energies.

TABLE I. Parameter setups

$\sqrt{s_{NN}}$ (GeV)	τ_0 (fm)	σ_{η_s}	σ_r (fm)	η/s	E_{sw} (GeV/fm ³)
200	0.4	0.6	0.6	0.08	0.65
62.4	0.6	0.6	0.6	0.08	0.6
39	0.8	0.4	0.6	0.08	0.55
27	1.0	0.4	0.4	0.10	0.5
19.6	1.2	0.2	0.4	0.12	0.45
7.7	2.0	0.2	0.3	0.16	0.35

C. Spin polarization

For a many-body system with fermions, the presence of fluid vorticity would polarize the spin of fermions due to the quantum mechanical spin-orbital coupling. At thermal equilibrium, the mean spin vector is determined by the local thermal vorticity, which at the leading order, is given by [12–14]:

$$S^\mu(x, p) = -\frac{1}{2m} \frac{S(S+1)}{3} [1 - f(x, p)] \epsilon^{\mu\nu\rho\sigma} p_\sigma \varpi_{\nu\rho}, \quad (6)$$

where S is the spin quantum number, m is the mass of fermion, $f(x, p)$ is the equilibrium Fermi-Dirac distribution function (In this spin polarization formula, the non-equilibrium corrections δf is neglected) and $\varpi_{\mu\nu}$ is the thermal vorticity defined as:

$$\varpi_{\mu\nu} = -\frac{1}{2} (\partial_\mu \beta_\nu - \partial_\nu \beta_\mu), \quad \text{with } \beta_\mu = u_\mu/T. \quad (7)$$

The spin polarization vector P^μ is defined as:

$$P^\mu(x, p) = \frac{1}{S} S^\mu(x, p). \quad (8)$$

With an average of $P^\mu(x, p)$ over the freeze-out hypersurface, the spin polarization in momentum space $P^\mu(p)$ is given by:

$$P^\mu(p) = \frac{\int d\Sigma_\nu p^\nu f(x, p) P^\mu(x, p)}{\int d\Sigma_\nu p^\nu f(x, p)}. \quad (9)$$

This is the spin Cooper-Frye formula which links the spin polarization of final hadrons in momentum space to the thermal vorticity on the freeze-out hypersurface [12–14].

The global spin polarization is obtained by integrating the numerator and denominator of Eq. (9) over the momentum:

$$P^\mu = \langle P^\mu(p) \rangle = \frac{\int \frac{d^3p}{E} \int d\Sigma_\nu p^\nu f(x, p) P^\mu(x, p)}{\int \frac{d^3p}{E} \int d\Sigma_\nu p^\nu f(x, p)}. \quad (10)$$

Note that the spin polarization measured in experiments is defined in the rest frame of the decay particle. To compare with experiment data, the expression of $P^\mu(x, p)$ or $S^\mu(x, p)$ is Lorentz transformed to particle's rest frame as follows:

$$S^* = S - \frac{p \cdot S}{E(E + m)} p. \quad (11)$$

Since the spin degree of freedom is not included in the dynamics of the hadronic transport model UrQMD [18, 59, 60]. In this work, we calculate the spin polarization on the freeze-out hypersurface E_{sw} according to Eqs. (6-11) without the UrQMD afterburner and the following spin polarization results are all for primary particles. For other soft hadron observables, such as the spectra and v_2 of identified hadrons shown in the Appendix A, the UrQMD afterburner is implemented.

III. RESULTS AND DISCUSSIONS

In this section, we implement AMPT+MUSIC hydrodynamic model to simulate the QGP fireball evolution and then use the spin Cooper-Frye formula described in Sec. II C to calculate and study the global and local spin polarization in 7.7 - 200 A GeV Au + Au collisions at RHIC. Here we also emphasize that with the parameter listed in table I and a UrQMD hadronic afterburner, this hybrid model can also nicely describe many soft hadron observables, such as the spectra and v_2 of identified hadrons. Please refer to the Appendix A for details.

A. Global spin polarization

Fig.1(a) shows the global spin polarization of primary Λ (without feed-down decay contributions) at mid-rapidity ($Y < 1$) along $-y$ direction. The calculated global Λ polarization from AMPT+MUSIC model decreases with the increase of collision energy and fits the experiment data within

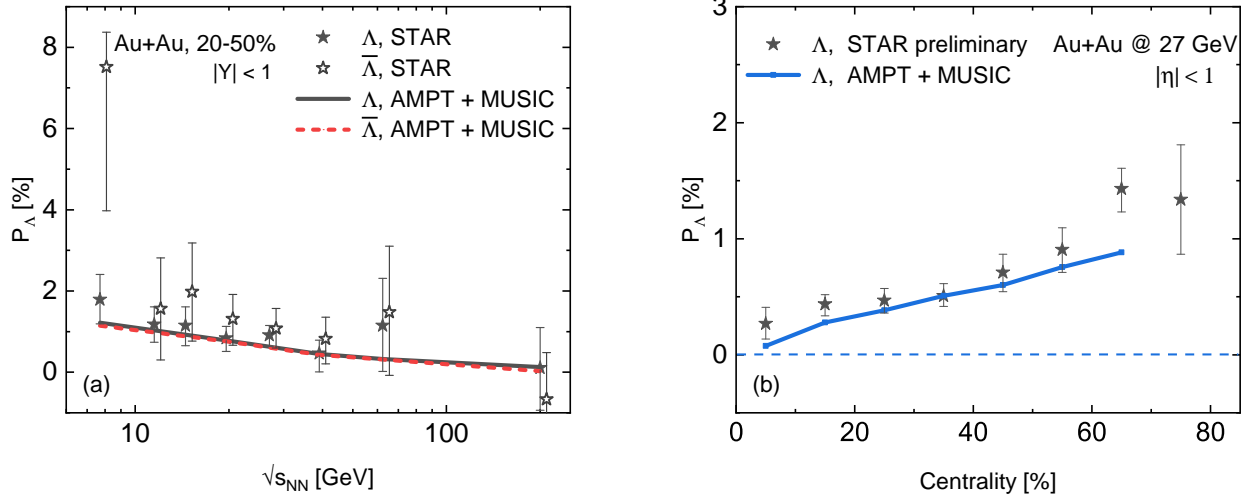


FIG. 1. (a) Global Λ polarization along the $-y$ direction as a function of collision energy. (b) Centrality dependence of global Λ polarization in 27 A GeV Au + Au collisions. The kinematic cut for the left and right panels are: $0.4 < p_T < 3$ GeV, $|Y| < 1$ and $0.4 < p_T < 3.0$ GeV, $|\eta| < 1$, respectively. The calculated spin polarization is for primary Λ and $\bar{\Lambda}$. The STAR data are taken from [4] (As the hyperon decay parameter α_Λ is updated, here and in the following figures, the published STAR results are scaled by a factor 0.87 [74]).

the error bars. The decreasing feature can be understood by the fact that, at mid-rapidity, the system behaves more likely to a boost-invariant fluid with smaller vorticity, although the total angular momentum is larger, at higher energy [75–77]. Figure 1(a) also shows that $P_{\bar{\Lambda}}$ is very close to P_Λ , since the difference between Λ and $\bar{\Lambda}$ in our calculation only comes from the finite baryon chemical potential μ_B in Eqs. (5) and (10). Although finite μ_B makes $P_{\bar{\Lambda}}$ larger than P_Λ , it also leads to more Λ production than $\bar{\Lambda}$ at earlier time, where the thermal vorticity effect is more significant [78]. These two effects cancel each other and makes P_Λ and $P_{\bar{\Lambda}}$ almost identical. For this reason, in the following calculations, we will only show results for Λ .

Fig. 1(b) shows the global Λ polarization as a function of centrality in 27 A GeV Au + Au collisions. Our calculation gives the same trend as the experimental measurements and almost fits the experimental data at different centralities. With the collision energy fixed, the global Λ polarization is positively correlated to the total angular momentum, which increases with the centrality.

In Fig. 2, we study the global spin polarization of Ξ^- (1322) and Ω^- (1672) with the purpose of providing a baseline for the studies of the magnetic moment, spin, and mass dependence of the spin polarization. The related spin ratios for these three baryons are $S_{\Omega^-} : S_{\Xi^-} : S_\Lambda = 3 : 1 : 1$ and the magnetic moment ratios are $|M_{\Omega^-}| : |M_{\Xi^-}| : |M_\Lambda| \approx 3 : 1 : 1$, while the mass ratios are $m_{\Omega^-} : m_{\Xi^-} : m_\Lambda = 1.5 : 1.2 : 1$. Therefore, by applying the spin Cooper-Frye formula Eq. (10), we expect a global-polarization ordering: $P_{\Omega^-} > P_{\Xi^-} \simeq P_\Lambda$, as demonstrated in Fig. 2. In our hydrodynamic calculations, the difference between the spin polarization of Ξ^- and Λ only comes from the mass difference in Eq. (10), which is too small to discern. Note that the spin polarizations of Ω^- and Ξ^0 were calculated in AMPT model in Ref. [24], in which a visible difference between Ξ^0 and Λ is seen. This

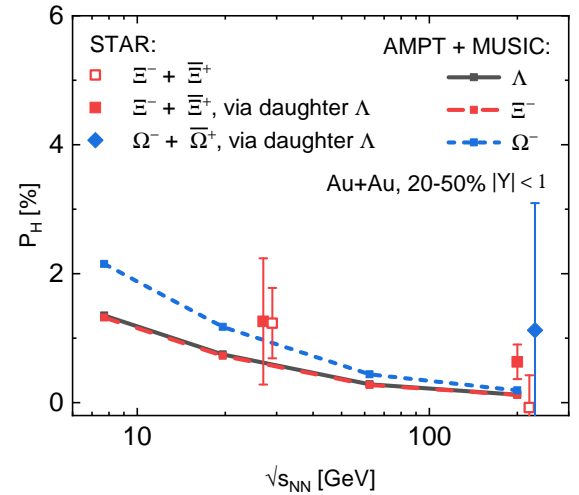


FIG. 2. Global spin polarization of Λ , Ξ^- , and Ω^- in Au+Au collisions at various collision energies. The kinematic setup is the same as Fig. 1. The STAR data are taken from Ref. [74]. For the measurements in 200 A GeV and 27 A GeV Au+Au collisions, the centrality is 20-80% and 20-50%, respectively. For the AMPT+MUSIC calculations, the centrality is 20-50%.

is probably due to that, in AMPT calculation of Ref. [24], the spin polarization depends also on the momentum distribution of the hyperons which are hadronized all the time rather than on specific particlization hypersurface. Nevertheless, in both the hydrodynamic and AMPT calculations, the global spin polarizations of Ξ and Λ are close to each other. For the spin-3/2 particle Ω^- , the spin polarization is clearly distinct from spin-1/2 Ξ^- and Λ . We emphasize that if a strong magnetic field is present (which is not taken into account in the current simulation), the spin Cooper-Frye formula is modified with

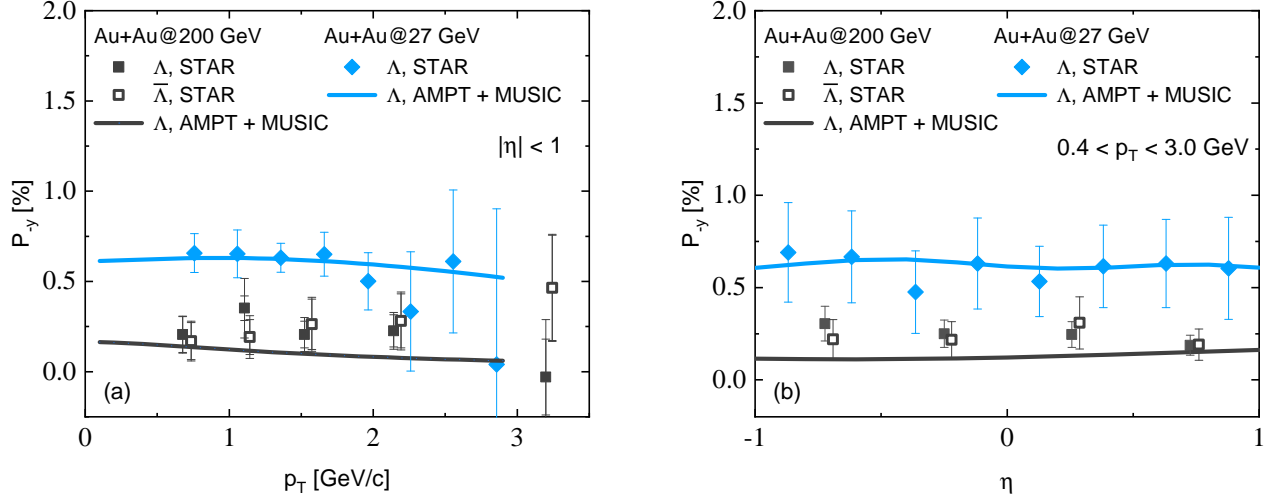


FIG. 3. (a) Transverse momentum and (b) pseudo-rapidity dependence of Λ polarization along $-y$ direction in 200 A GeV Au + Au collisions at 20-60% centrality and in 27 A GeV Au + Au collisions at 15-75% centrality. The STAR data are taken from [5, 79].

the replacement $\varpi_{\rho\sigma} \rightarrow \varpi_{\rho\sigma} + M_H F_{\rho\sigma}/(ST)$ with M_H the magnetic moment of hyperon H , S the spin quantum number of H , and $F_{\rho\sigma}$ the electromagnetic field [17]. Since the ratios of the magnetic moment over spin for Ω^- , Λ , and Ξ^- are roughly the same, the magnetic-field induced polarization would be also similar. Besides, the magnetic field can also induce splitting of the spin polarization between hyperons and anti-hyperons [80]. (See e.g. Ref. [81] for another possible explanation of hyperon and anti-hyperon spin polarization splitting.) Currently, the preliminary experimental data shown in Fig. 2 have large error bars. Even precise measurements in the future, when compared with our current results, may provide a novel access to the detection of the magnetic fields at freeze-out in heavy-ion collisions.

B. Local spin polarization

After studying the global spin polarization, we now focus on the local spin polarization, namely, the differential properties of the spin polarization. Figure 3 shows the transverse momentum and pseudo-rapidity dependent Λ polarization. AMPT+MUSIC calculations show no significant dependence on p_T or η , which qualitatively describe the experimental data in 200 A GeV and 27 A GeV Au+Au collisions [5, 79].

Besides the mid-rapidity results, forward and backward spin polarization provide more nuanced information for the local vortical structure. Fig. 4(a) shows the local Λ polarization in y direction, P_y , distributed in the p_x - Y plane. At finite rapidity region, P_y shows opposite signs on two sides of the longitudinal axis and form a quadrupole structure in the p_x - Y plane. As Refs. [24, 82, 83] pointed out, this quadrupole pattern is a projection of a ring structure of the transverse spin polarization $\mathbf{P}_\perp = (P_x, P_y)$ onto p_x - Y plane at forward or backward region. Fig. 4(c) and Fig. 4(d) show such a ring structure of \mathbf{P}_\perp at forward and backward rapidity $Y = \pm 2$,

where the direction of the ring depends on the sign of rapidity. In the mid-rapidity region, the global spin polarization degenerates to direct at $-y$ direction evenly, as shown in Fig. 4(b). Physically, the ring structure of \mathbf{P}_\perp at finite rapidity is understood by the ring structure of thermal vorticity at finite spacetime rapidity due to the anisotropic and inhomogeneous expansion of the system. For more discussions, please refer to Refs. [24, 83].

Figure 4 also demonstrates that the transverse spin polarization has striking angular distribution at different rapidity. To visualize such angular distribution more clearly, we decompose \mathbf{P}_\perp into radial (r) and azimuthal (ϕ) components and show their azimuthal-angle dependence in Fig. 5. The special modulation feature in ϕ is clearly seen, which could provide an specific way to detect the vortex-ring structure by measuring such ϕ -modulation behavior of radial, P_r , and azimuthal, P_ϕ , components of \mathbf{P}_\perp at finite rapidity.

Fig. 6(a) shows the azimuthal dependence of Λ polarization P_{-y} measured in experiment and calculated by model. Our calculated P_{-y} slightly increases with the azimuthal angle ϕ from 0 to $\pi/2$, while, the measured P_{-y} shows an opposite trend and decreases with ϕ , which is strong at the in-plane direction but almost vanished at the out-of-plane direction. Fig. 6(b) shows P_z calculated from our model and compared with the $\langle \cos(\theta_p^*) \rangle^{\text{sub}}$ measured in experiment. Note that $\langle \cos(\theta_p^*) \rangle^{\text{sub}}$ is related to the longitudinal polarization by $P_z = \frac{\langle \cos(\theta_p^*) \rangle^{\text{sub}}}{\alpha_H \langle \cos^2(\theta_p^*) \rangle^{\text{sub}}}$, where α_H is the decay factor and $\langle \dots \rangle^{\text{sub}}$ denotes the subtraction of the acceptance effect in experiment. As demonstrated by the lower panels of Fig. 7, the distribution of longitudinal spin polarization P_z in the p_x - p_y transverse momentum plane from our model calculations shows an obvious quadrupole structure. While Fig. 6(b) illustrates that although both model and data present a quadrupole pattern, the sign is opposite. Such situations are similar to many hydrodynamics or transport model calculations based on the

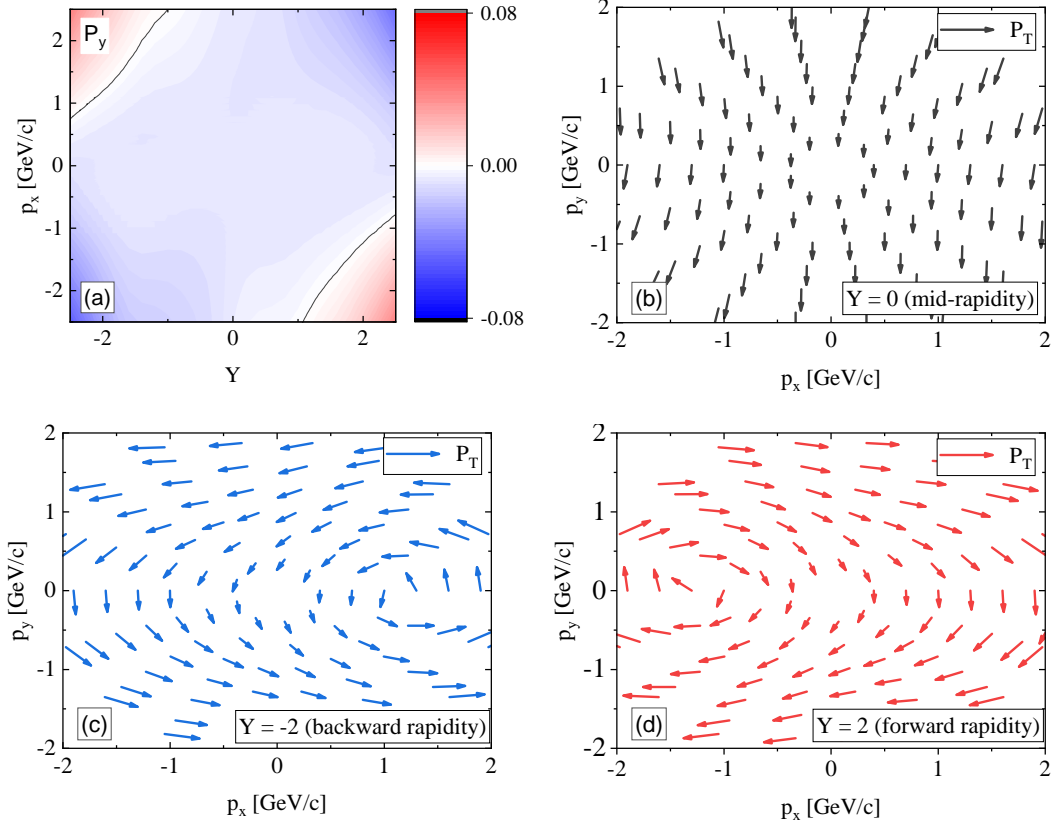


FIG. 4. (a) Distribution of P_y on p_x - Y plane in momentum space. (b-d) Transverse spin polarization \mathbf{P}_\perp at mid-rapidity ($Y = 0$), at backward rapidity ($Y = -2$), and at forward rapidity ($Y = 2$) in 19.6 A GeV Au + Au collisions at 20-50% centrality, calculated from AMPT+MUSIC.

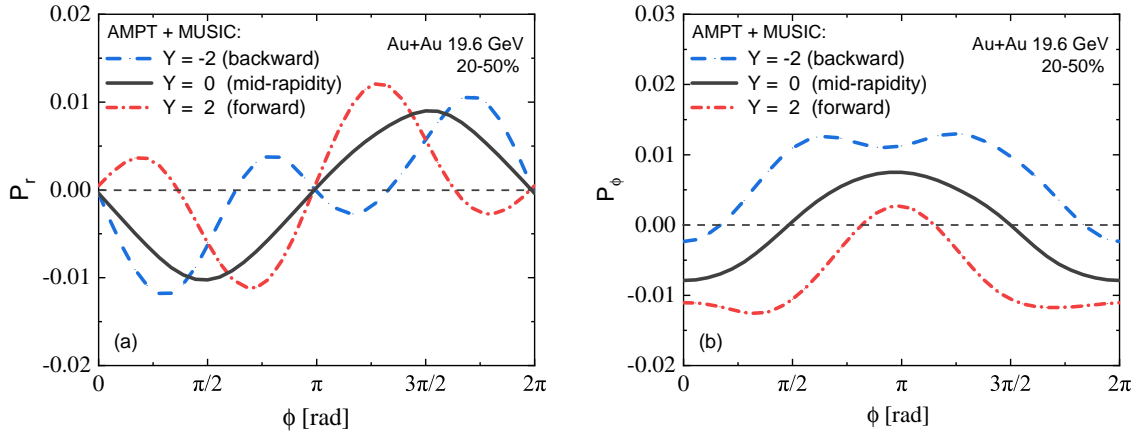


FIG. 5. The azimuthal-angle ϕ dependence of the (a) radial (r) and (b) azimuthal (ϕ) components of the transverse spin polarization \mathbf{P}_\perp in momentum space at forward, backward, and mid rapidity, calculated from AMPT+MUSIC.

spin Cooper-Frye formula, which could successfully describe the magnitude and energy dependence of the global Λ polarization [15–24], but fail to reproduce the local spin polarization, namely, the azimuthal dependence of P_{-y} and P_z . This is the challenging spin “sign problem” which has attracted a lot of attention but has not been solved till now (For recent

development, please refer to Refs. [26–32].

The spin Cooper-Frye formula (9) used in this paper and early calculations can be regarded as a mapping between thermal vorticity in coordinate space to spin polarization in momentum space, where the thermal vorticity is mainly contributed from the initial condition and the hydrodynamic evo-

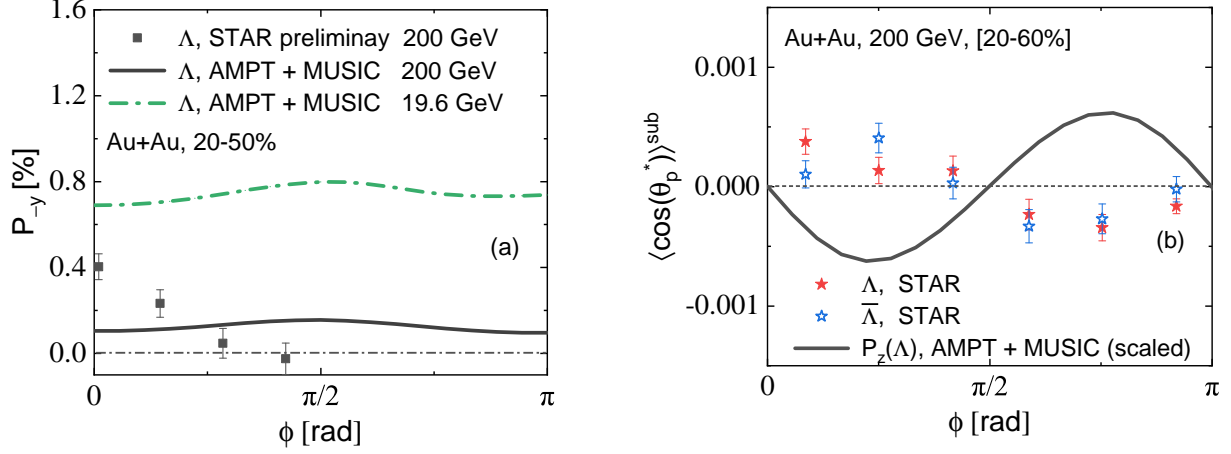


FIG. 6. Azimuthal distribution of (a) P_y and (b) $\langle \cos(\theta_p^*) \rangle^{\text{sub}}$ in 200 A GeV and 19.6 A GeV Au + Au collisions at 20-50% centrality. In sub-figure (b), the calculated P_z is scaled by a factor 0.33 to make the comparison more explicit. The STAR data are taken from [6, 8].

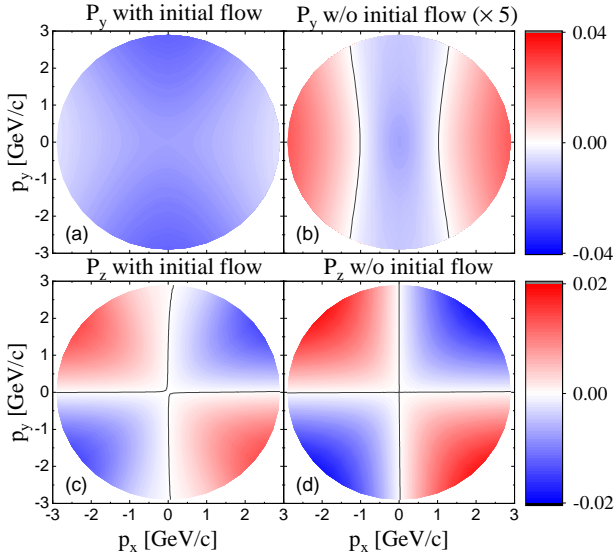


FIG. 7. The distribution of P_y and P_z at mid-rapidity in transverse p_x - p_y plane in 19.6 A GeV Au + Au collisions, calculated from AMPT+MUSIC with and without initial flow.

lution. Since the initial condition imprints the total angular momentum of the system, it also largely influences the global spin polarization in the final state due to the angular momentum conservation. In contrast, both the initial condition and hydrodynamic evolution could largely affect the local spin polarization, which reflect the vorticity structure at late stage evolution.

In Fig. 7, we plot the transverse distribution of spin polarization P_y and P_z in 20-50% Au + Au collision at mid-rapidity, calculated from AMPT+MUSIC with and without initial flow. The full AMPT initial condition with initial flow has been described in Sec. II A. For the AMPT initial condi-

tion without initial flow, we directly set $u^x(\tau_0) = u^y(\tau_0) = u^{\eta_s}(\tau_0) = 0$ and obtain the initial energy density as described in [61]. The initial flow directly influences the initial angular momentum of the created QGP fireball. When it is turned off, the vorticity of the initial fluid reduces to almost zero value. Correspondingly, the final global polarization P_y almost vanishes, as demonstrated in Fig. 7(b) (Note that we re-scaled the result of P_y without initial flow by a factor of 5 to make it visible.).

It is generally believed that the longitudinal polarization P_z is directly associated with the anisotropic transverse expansion of the systems but insensitive to the initial angular momentum [26]. This is confirmed by our AMPT+MUSIC calculations with and without initial flow, which demonstrate that P_z has similar structure in these two comparison runs, as shown by the lower panels of Fig. 7. This also means that the longitudinal vorticity P_z mainly probes the vortical structure developed during the hydrodynamic evolution.

Note that, according to Eqs. (6)-(10), the longitudinal component P_z is contributed by 3 parts :

$$P_z(p) \sim p^t \varpi_{xy} + p^x \varpi_{ty} - p^y \varpi_{tx}. \quad (12)$$

The first term is related to the non-relativistic vorticity $\omega_z \sim (\nabla \times \mathbf{v})_z$, which arises when the system expands anisotropically. The second and third terms are relativistic effect and can be considered as Thomas precession $\omega_{\text{Tho}}^z \sim (\mathbf{p} \times \mathbf{a})^z / m$ (taking into account the fact that for nearly ideal fluid $\mathbf{a} \approx -T^{-1} \nabla T$) with \mathbf{a} the acceleration of the fluid. Figure 8 shows that the contributions from the last two terms are much bigger than the first term, which indicates that the spin “sign problem” is possibly a relativistic effect. Such analysis works for all the hydrodynamic or transport calculations of P_z based on the spin Cooper-Frye formula with thermal vorticity as the spin chemical potential. Similar analysis were also discussed in Ref. [89]. The discrepancy between the theoretical calculations based on the spin Cooper-Frye formula and the exper-

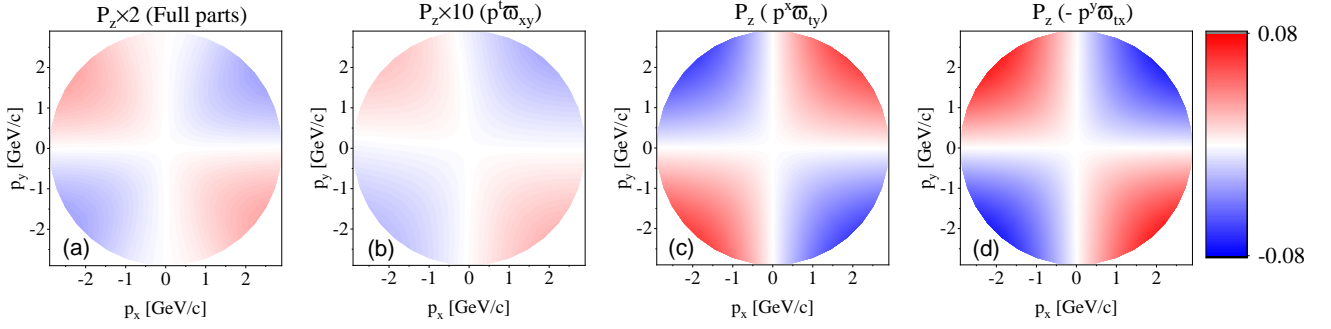


FIG. 8. Contributions of P_z from AMPT+MUSIC calculations: (a) total P_z , (b) the non-relativistic contribution, (c) and (d) Thomas-precession contributions in Eq. (12).

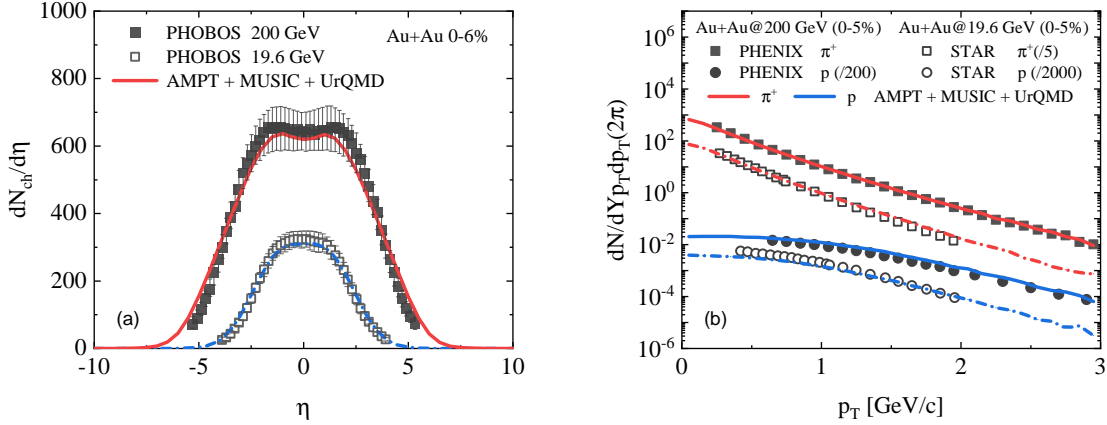


FIG. 9. (a) Pseudo-rapidity distribution of all charged hadron and (b) transverse momentum spectra of pions and protons in 200 and 19.6 GeV Au+Au collisions. The experimental data are from the PHOBOS, PHENIX, and STAR Collaborations [84–86].

imental data is still not fully understood. Some attempts to resolve such problem can be found in Refs. [27–32].

IV. SUMMARY

In this paper, we used MUSIC viscous hydrodynamics with the AMPT pre-equilibrium dynamics to study the hyperon spin polarization in relativistic heavy-ion collisions. With a UrQMD hadron cascade afterburner, this hybrid model can nicely describe various soft hadron observables at RHIC-BES energies, such as the rapidity distribution of all charged hadrons, transverse momentum spectra, and differential elliptic flows of identified hadrons; see Appendix A for the details. In order to study the spin polarization of hyperons, we implemented the spin Cooper-Frye formula that associates the momentum-space distribution of the hyperon polarization with the position-space vorticity of the fluid, and obtained a nice description of the collision-energy dependence, centrality dependence, and the p_T and η dependence of the Λ polarization. We also studied and predicted the global spin polarization of Ξ^- and Ω^- as a function of collision energy, which provides a baseline for the studies of the magnetic moment, spin, and mass dependence of the spin polarization.

For the local spin polarization, we calculated the radial and azimuthal components of the transverse Λ polarization and found specific modulating behavior that could reflect the circular vortical structure. However, for the azimuthal dependence of the transverse and the longitudinal spin polarization, our approach, like most of the previous theoretical calculations, gives an opposite trend compared with the experimental data. These results suggest that the spin Cooper-Frye formula, which was derived under the assumption of thermal equilibrium of spin degree of freedom, needs to be improved. A promising direction for such a purpose is the spin hydrodynamics which has been intensively discussed recently [90–97]. With the future numerical implementation, such framework might give important insight to the puzzle of local spin polarization and may also be used to study the global and local spin alignment of vector mesons [39–42].

Appendix A: Soft hadronic observables

In this appendix, we check the soft hadronic observables from AMPT + MUSIC simulations which serve as baseline calculations before study the spin-polarization in relativistic heavy ion collisions. Figures 9 and 10 present the rapidity dis-

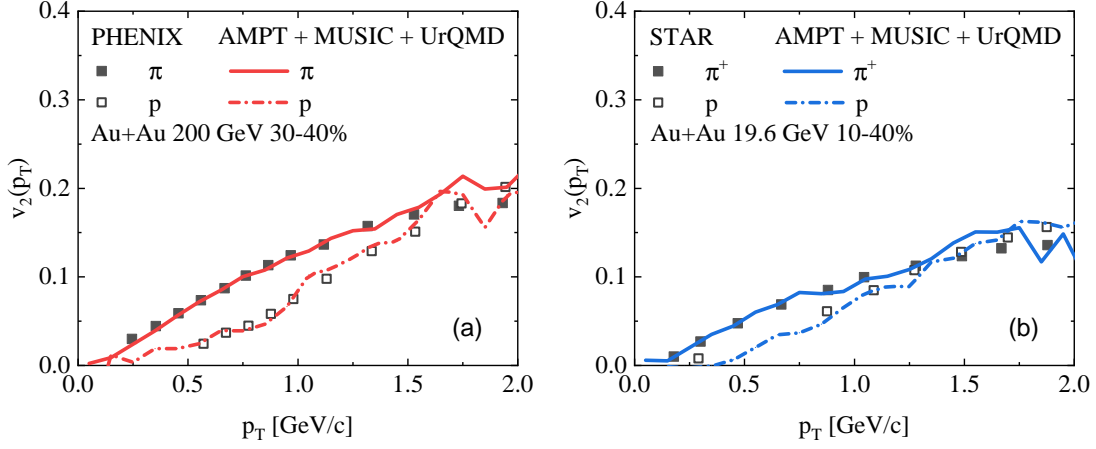


FIG. 10. Differential elliptic flow $v_2(p_T)$ of pions and protons in 200 A GeV and 19.6 A GeV Au+Au collisions. The experimental data are from PHENIX and STAR Collaborations [87, 88].

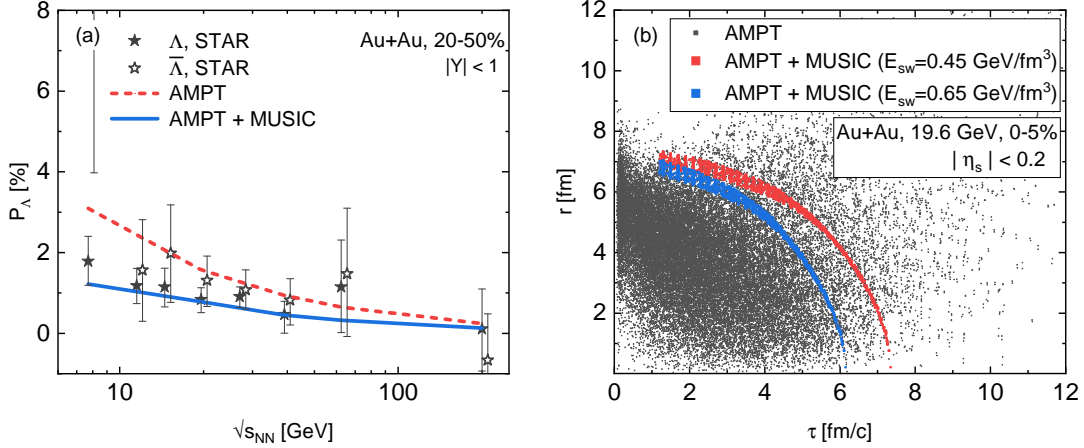


FIG. 11. (a) Energy dependent global Λ polarization, calculated from AMPT [24], and from AMPT + MUSIC. (b) Hadronization distribution from AMPT and the freeze-out hypersurface from AMPT+MUSIC hydrodynamic model.

tribution of all charged hadrons, transverse momentum spectra and differential elliptic flow of pions and protons in 200 A GeV and 19.6 A GeV Au+Au collisions. With a UrQMD hadronic afterburner and properly tuned parameters listed in Table I, our AMPT + MUSIC simulations nicely fit these soft observables measured in experiment. These agreements indicate that our hybrid model give a nice description for the bulk evolution of the QGP fireball.

Appendix B: Global spin polarization — a comparison between AMPT and AMPT+MUSIC

In this appendix, we compare the global spin polarization calculated from our AMPT+MUSIC hybrid model and from the pure transport approach AMPT. As shown in Fig. 11(a), the global polarization from AMPT is larger than that from MUSIC, although the pre-equilibrium dynamics at the early stage are both provided by AMPT.

To understand the difference between these two results, in Fig. 11(b), we compare the hadronization distribution in AMPT and the freeze-out hypersurface from AMPT+MUSIC hydrodynamic model. For hydrodynamic simulations, the particlization happens on the freeze-out hypersurface with constant energy density. For AMPT simulation, the hadronization process is realized through parton recombination with the Monte-Carlo sampling [57]. As a result, the hadronization in AMPT happens all the time during the system evolution. In contrast, the hydrodynamic particlization happens at a specific freeze-out hypersurface, which, on average, happens later than the AMPT hadronization. Noting that the thermal vorticity gradually decreases with the evolution, AMPT thus gives a larger global polarization than the hydrodynamic simulations.

ACKNOWLEDGMENTS

We thank T. Nidda, Z.-W. Lin, D.-X. Wei, and X.-L. Xia for helpful discussions. The work of B. F. K. X. and H. S. is supported by are supported by the NSFC under grant Nos. 11675004 and No. 12075007. The work of X. G. H is supported by NSFC through Grants No. 11535012 and

No. 11675041. B. F. K. X. and H. S. also gratefully acknowledge the extensive computing resources provided by the Super-computing Center of Chinese Academy of Science (SCCAS), Tianhe-1A from the National Supercomputing Center in Tianjin, China and the High-performance Computing Platform of Peking University.

-
- [1] Z.-T. Liang and X.-N. Wang, *Phys. Rev. Lett.* **94**, 102301 (2005), [Erratum: *Phys.Rev.Lett.* 96, 039901 (2006)], [arXiv:nucl-th/0410079](#).
 - [2] S. A. Voloshin, (2004), [arXiv:nucl-th/0410089](#).
 - [3] B. Abelev *et al.* (STAR), *Phys. Rev. C* **76**, 024915 (2007), [Erratum: *Phys.Rev.C* 95, 039906 (2017)], [arXiv:0705.1691 \[nucl-ex\]](#).
 - [4] L. Adamczyk *et al.* (STAR), *Nature* **548**, 62 (2017), [arXiv:1701.06657 \[nucl-ex\]](#).
 - [5] J. Adam *et al.* (STAR), *Phys. Rev. C* **98**, 014910 (2018), [arXiv:1805.04400 \[nucl-ex\]](#).
 - [6] T. Niida (STAR), *Nucl. Phys. A* **982**, 511 (2019), [arXiv:1808.10482 \[nucl-ex\]](#).
 - [7] S. Acharya *et al.* (ALICE), *Phys. Rev. C* **101**, 044611 (2020), [arXiv:1909.01281 \[nucl-ex\]](#).
 - [8] J. Adam *et al.* (STAR), *Phys. Rev. Lett.* **123**, 132301 (2019), [arXiv:1905.11917 \[nucl-ex\]](#).
 - [9] J.-H. Gao, S.-W. Chen, W.-T. Deng, Z.-T. Liang, Q. Wang, and X.-N. Wang, *Phys. Rev. C* **77**, 044902 (2008), [arXiv:0710.2943 \[nucl-th\]](#).
 - [10] B. Betz, M. Gyulassy, and G. Torrieri, *Phys. Rev. C* **76**, 044901 (2007), [arXiv:0708.0035 \[nucl-th\]](#).
 - [11] X.-G. Huang, P. Huovinen, and X.-N. Wang, *Phys. Rev. C* **84**, 054910 (2011), [arXiv:1108.5649 \[nucl-th\]](#).
 - [12] F. Becattini, V. Chandra, L. Del Zanna, and E. Grossi, *Annals Phys.* **338**, 32 (2013), [arXiv:1303.3431 \[nucl-th\]](#).
 - [13] R.-h. Fang, L.-g. Pang, Q. Wang, and X.-n. Wang, *Phys. Rev. C* **94**, 024904 (2016), [arXiv:1604.04036 \[nucl-th\]](#).
 - [14] Y.-C. Liu, K. Mameda, and X.-G. Huang, *Chin. Phys. C* **44**, 094101 (2020), [arXiv:2002.03753 \[hep-ph\]](#).
 - [15] F. Becattini, L. Csernai, and D. Wang, *Phys. Rev. C* **88**, 034905 (2013), [Erratum: *Phys.Rev.C* 93, 069901 (2016)], [arXiv:1304.4427 \[nucl-th\]](#).
 - [16] F. Becattini, G. Inghirami, V. Rolando, A. Beraudo, L. Del Zanna, A. De Pace, M. Nardi, G. Pagliara, and V. Chandra, *Eur. Phys. J. C* **75**, 406 (2015), [Erratum: *Eur.Phys.J.C* 78, 354 (2018)], [arXiv:1501.04468 \[nucl-th\]](#).
 - [17] F. Becattini, I. Karpenko, M. Lisa, I. Upsal, and S. Voloshin, *Phys. Rev. C* **95**, 054902 (2017), [arXiv:1610.02506 \[nucl-th\]](#).
 - [18] I. Karpenko and F. Becattini, *Eur. Phys. J. C* **77**, 213 (2017), [arXiv:1610.04717 \[nucl-th\]](#).
 - [19] Y. Xie, M. Bleicher, H. Stöcker, D. Wang, and L. Csernai, *Phys. Rev. C* **94**, 054907 (2016), [arXiv:1610.08678 \[nucl-th\]](#).
 - [20] Y. Xie, D. Wang, and L. P. Csernai, *Phys. Rev. C* **95**, 031901 (2017), [arXiv:1703.03770 \[nucl-th\]](#).
 - [21] H. Li, L.-G. Pang, Q. Wang, and X.-L. Xia, *Phys. Rev. C* **96**, 054908 (2017), [arXiv:1704.01507 \[nucl-th\]](#).
 - [22] Y. B. Ivanov, V. Toneev, and A. Soldatov, *Phys. Rev. C* **100**, 014908 (2019), [arXiv:1903.05455 \[nucl-th\]](#).
 - [23] S. Shi, K. Li, and J. Liao, *Phys. Lett. B* **788**, 409 (2019), [arXiv:1712.00878 \[nucl-th\]](#).
 - [24] D.-X. Wei, W.-T. Deng, and X.-G. Huang, *Phys. Rev. C* **99**, 014905 (2019), [arXiv:1810.00151 \[nucl-th\]](#).
 - [25] Y. Ivanov and A. Soldatov, *Phys. Rev. C* **102**, 024916 (2020), [arXiv:2004.05166 \[nucl-th\]](#).
 - [26] F. Becattini and I. Karpenko, *Phys. Rev. Lett.* **120**, 012302 (2018), [arXiv:1707.07984 \[nucl-th\]](#).
 - [27] W. Florkowski, A. Kumar, R. Ryblewski, and A. Mazeliauskas, *Phys. Rev. C* **100**, 054907 (2019), [arXiv:1904.00002 \[nucl-th\]](#).
 - [28] H.-Z. Wu, L.-G. Pang, X.-G. Huang, and Q. Wang, *Phys. Rev. Research* **1**, 033058 (2019), [arXiv:1906.09385 \[nucl-th\]](#).
 - [29] Y. Xie, D. Wang, and L. P. Csernai, *Eur. Phys. J. C* **80**, 39 (2020), [arXiv:1907.00773 \[hep-ph\]](#).
 - [30] X.-L. Xia, H. Li, X.-G. Huang, and H. Z. Huang, *Phys. Rev. C* **100**, 014913 (2019), [arXiv:1905.03120 \[nucl-th\]](#).
 - [31] F. Becattini, G. Cao, and E. Speranza, *Eur. Phys. J. C* **79**, 741 (2019), [arXiv:1905.03123 \[nucl-th\]](#).
 - [32] S. Y. Liu, Y. Sun, and C. M. Ko, *Phys. Rev. Lett.* **125**, 062301 (2020), [arXiv:1910.06774 \[nucl-th\]](#).
 - [33] X.-G. Huang, (2020), [arXiv:2002.07549 \[nucl-th\]](#).
 - [34] Y.-C. Liu and X.-G. Huang, *Nucl. Sci. Tech.* **31**, 56 (2020), [arXiv:2003.12482 \[nucl-th\]](#).
 - [35] F. Becattini and M. A. Lisa, (2020), [10.1146/annurev-nucl-021920-095245](#), [arXiv:2003.03640 \[nucl-ex\]](#).
 - [36] J.-H. Gao, G.-L. Ma, S. Pu, and Q. Wang, *Nucl. Sci. Tech.* **31**, 90 (2020), [arXiv:2005.10432 \[hep-ph\]](#).
 - [37] J.-H. Gao, Z.-T. Liang, Q. Wang, and X.-N. Wang, (2020), [arXiv:2009.04803 \[nucl-th\]](#).
 - [38] X.-G. Huang, J. Liao, Q. Wang, and X.-L. Xia, (2020), [arXiv:2010.08937 \[nucl-th\]](#).
 - [39] Z.-T. Liang and X.-N. Wang, *Phys. Lett. B* **629**, 20 (2005), [arXiv:nucl-th/0411101](#).
 - [40] X.-L. Sheng, L. Oliva, and Q. Wang, *Phys. Rev. D* **101**, 096005 (2020), [arXiv:1910.13684 \[nucl-th\]](#).
 - [41] X.-L. Sheng, Q. Wang, and X.-N. Wang, *Phys. Rev. D* **102**, 056013 (2020), [arXiv:2007.05106 \[nucl-th\]](#).
 - [42] X.-L. Xia, H. Li, X.-G. Huang, and H. Z. Huang, (2020), [arXiv:2010.01474 \[nucl-th\]](#).
 - [43] H. Taya *et al.* (ExHIC-P), *Phys. Rev. C* **102**, 021901 (2020), [arXiv:2002.10082 \[nucl-th\]](#).
 - [44] S. Y. Liu and Y. Yin, (2020), [arXiv:2006.12421 \[nucl-th\]](#).
 - [45] B. Schenke, S. Jeon, and C. Gale, *Phys. Rev. Lett.* **106**, 042301 (2011), [arXiv:1009.3244 \[hep-ph\]](#).
 - [46] B. Schenke, S. Jeon, and C. Gale, *Phys. Rev. C* **85**, 024901 (2012), [arXiv:1109.6289 \[hep-ph\]](#).
 - [47] C. Gale, S. Jeon, B. Schenke, P. Tribedy, and R. Venugopalan, *Phys. Rev. Lett.* **110**, 012302 (2013), [arXiv:1209.6330 \[nucl-th\]](#).
 - [48] B. Schenke and R. Venugopalan, *Phys. Rev. Lett.* **113**, 102301 (2014), [arXiv:1405.3605 \[nucl-th\]](#).
 - [49] I. Karpenko, P. Huovinen, H. Petersen, and M. Bleicher, *Phys. Rev. C* **91**, 064901 (2015), [arXiv:1502.01978 \[nucl-th\]](#).
 - [50] H. Song, Y. Zhou, and K. Gajdosova, *Nucl. Sci. Tech.* **28**, 99 (2017), [arXiv:1703.00670 \[nucl-th\]](#).

- [51] W. Zhao, H.-j. Xu, and H. Song, *Eur. Phys. J. C* **77**, 645 (2017), [arXiv:1703.10792 \[nucl-th\]](#).
- [52] X. Zhu, Y. Zhou, H. Xu, and H. Song, *Phys. Rev. C* **95**, 044902 (2017), [arXiv:1608.05305 \[nucl-th\]](#).
- [53] W. Zhao, L. Zhu, H. Zheng, C. M. Ko, and H. Song, *Phys. Rev. C* **98**, 054905 (2018), [arXiv:1807.02813 \[nucl-th\]](#).
- [54] G. S. Denicol, C. Gale, S. Jeon, A. Monnai, B. Schenke, and C. Shen, *Phys. Rev. C* **98**, 034916 (2018), [arXiv:1804.10557 \[nucl-th\]](#).
- [55] B. Schenke, C. Shen, and P. Tribedy, (2020), [arXiv:2005.14682 \[nucl-th\]](#).
- [56] B. Schenke, C. Shen, and P. Tribedy, *Phys. Lett. B* **803**, 135322 (2020), [arXiv:1908.06212 \[nucl-th\]](#).
- [57] Z.-W. Lin, C. M. Ko, B.-A. Li, B. Zhang, and S. Pal, *Phys. Rev. C* **72**, 064901 (2005), [arXiv:nucl-th/0411110](#).
- [58] B. Schenke, S. Jeon, and C. Gale, *Phys. Rev. C* **82**, 014903 (2010), [arXiv:1004.1408 \[hep-ph\]](#).
- [59] S. Bass *et al.*, *Prog. Part. Nucl. Phys.* **41**, 255 (1998), [arXiv:nucl-th/9803035](#).
- [60] M. Bleicher *et al.*, *J. Phys. G* **25**, 1859 (1999), [arXiv:hep-ph/9909407](#).
- [61] H.-j. Xu, Z. Li, and H. Song, *Phys. Rev. C* **93**, 064905 (2016), [arXiv:1602.02029 \[nucl-th\]](#).
- [62] W. Zhao, Y. Zhou, H. Xu, W. Deng, and H. Song, *Phys. Lett. B* **780**, 495 (2018), [arXiv:1801.00271 \[nucl-th\]](#).
- [63] W. Zhao, Y. Zhou, K. Murase, and H. Song, *Eur. Phys. J. C* **80**, 846 (2020), [arXiv:2001.06742 \[nucl-th\]](#).
- [64] X.-N. Wang and M. Gyulassy, *Phys. Rev. D* **44**, 3501 (1991).
- [65] M. Gyulassy and X.-N. Wang, *Comput. Phys. Commun.* **83**, 307 (1994), [arXiv:nucl-th/9502021](#).
- [66] L. Pang, Q. Wang, and X.-N. Wang, *Phys. Rev. C* **86**, 024911 (2012), [arXiv:1205.5019 \[nucl-th\]](#).
- [67] L.-G. Pang, H. Petersen, Q. Wang, and X.-N. Wang, *Phys. Rev. Lett.* **117**, 192301 (2016), [arXiv:1605.04024 \[hep-ph\]](#).
- [68] G. Denicol, H. Niemi, E. Molnar, and D. Rischke, *Phys. Rev. D* **85**, 114047 (2012), [Erratum: *Phys. Rev. D* **91**, 039902 (2015)], [arXiv:1202.4551 \[nucl-th\]](#).
- [69] G. Denicol, S. Jeon, and C. Gale, *Phys. Rev. C* **90**, 024912 (2014), [arXiv:1403.0962 \[nucl-th\]](#).
- [70] S. Ryu, J. F. Paquet, C. Shen, G. Denicol, B. Schenke, S. Jeon, and C. Gale, *Phys. Rev. Lett.* **115**, 132301 (2015), [arXiv:1502.01675 \[nucl-th\]](#).
- [71] C. Shen, Z. Qiu, H. Song, J. Bernhard, S. Bass, and U. Heinz, *Comput. Phys. Commun.* **199**, 61 (2016), [arXiv:1409.8164 \[nucl-th\]](#).
- [72] F. Cooper and G. Frye, *Phys. Rev. D* **10**, 186 (1974).
- [73] H. Grad, *Communications on Pure and Applied Mathematics* **2**, 331 (1949), <https://onlinelibrary.wiley.com/doi/pdf/10.1002/cpa.3160020403>.
- [74] J. Adams (STAR), “Global polarization of hyperons from STAR experiment,” Talk given at RHIC and AGS Annual Users Meeting 2020 (2020).
- [75] W.-T. Deng and X.-G. Huang, *Phys. Rev. C* **93**, 064907 (2016), [arXiv:1603.06117 \[nucl-th\]](#).
- [76] Y. Jiang, Z.-W. Lin, and J. Liao, *Phys. Rev. C* **94**, 044910 (2016), [Erratum: *Phys. Rev. C* **95**, 049904 (2017)], [arXiv:1602.06580 \[hep-ph\]](#).
- [77] X.-G. Deng, X.-G. Huang, Y.-G. Ma, and S. Zhang, *Phys. Rev. C* **101**, 064908 (2020), [arXiv:2001.01371 \[nucl-th\]](#).
- [78] B. Fu, K. Xu, X.-G. Huang, and H. Song, *private notes*.
- [79] J. Adams (STAR), “Differential measurements of Lambda polarization in Au + Au collisions and a search for the magnetic field by STAR,” Talk given at Quark Matter Conference (2019).
- [80] Y. Guo, S. Shi, S. Feng, and J. Liao, *Phys. Lett. B* **798**, 134929 (2019), [arXiv:1905.12613 \[nucl-th\]](#).
- [81] V. E. Ambrus and M. Cherdub, (2020), [arXiv:2010.05831 \[hep-ph\]](#).
- [82] Y. B. Ivanov and A. Soldatov, *Phys. Rev. C* **97**, 044915 (2018), [arXiv:1803.01525 \[nucl-th\]](#).
- [83] X.-L. Xia, H. Li, Z.-B. Tang, and Q. Wang, *Phys. Rev. C* **98**, 024905 (2018), [arXiv:1803.00867 \[nucl-th\]](#).
- [84] B. Back *et al.*, *Phys. Rev. Lett.* **91**, 052303 (2003), [arXiv:nucl-ex/0210015](#).
- [85] L. Adamczyk *et al.* (STAR), *Phys. Rev. C* **96**, 044904 (2017), [arXiv:1701.07065 \[nucl-ex\]](#).
- [86] S. Adler *et al.* (PHENIX), *Phys. Rev. C* **69**, 034909 (2004), [arXiv:nucl-ex/0307022](#).
- [87] A. Adare *et al.* (PHENIX), *Phys. Rev. C* **92**, 034913 (2015), [arXiv:1412.1043 \[nucl-ex\]](#).
- [88] L. Adamczyk *et al.* (STAR), *Phys. Rev. C* **93**, 014907 (2016), [arXiv:1509.08397 \[nucl-ex\]](#).
- [89] I. Karpenko and F. Becattini, *Nucl. Phys. A* **982**, 519 (2019), [arXiv:1811.00322 \[nucl-th\]](#).
- [90] W. Florkowski, B. Friman, A. Jaiswal, and E. Speranza, *Phys. Rev. C* **97**, 041901 (2018), [arXiv:1705.00587 \[nucl-th\]](#).
- [91] K. Hattori, M. Hongo, X.-G. Huang, M. Matsuo, and H. Taya, *Phys. Lett. B* **795**, 100 (2019), [arXiv:1901.06615 \[hep-th\]](#).
- [92] D. Montenegro and G. Torrieri, *Phys. Rev. D* **100**, 056011 (2019), [arXiv:1807.02796 \[hep-th\]](#).
- [93] W. Florkowski, A. Kumar, and R. Ryblewski, *Prog. Part. Nucl. Phys.* **108**, 103709 (2019), [arXiv:1811.04409 \[nucl-th\]](#).
- [94] S. Bhadury, W. Florkowski, A. Jaiswal, A. Kumar, and R. Ryblewski, (2020), [arXiv:2002.03937 \[hep-ph\]](#).
- [95] S. Bhadury, W. Florkowski, A. Jaiswal, A. Kumar, and R. Ryblewski, (2020), [arXiv:2008.10976 \[nucl-th\]](#).
- [96] S. Shi, C. Gale, and S. Jeon, (2020), [arXiv:2008.08618 \[nucl-th\]](#).
- [97] K. Fukushima and S. Pu, (2020), [arXiv:2010.01608 \[hep-th\]](#).